Applied Surface Science 401 (2017) 297–305

Contents lists available at ScienceDirect

Applied Surface Science

journal homepage: www.elsevier.com/locate/apsusc

Full length article

Highly effective surface-enhanced fluorescence substrates with roughened 3D flowerlike silver nanostructures fabricated in liquid crystalline phase

Ying Zhang[a,b], Chengliang Yang[a,*], Xiangjun Xiang[a,b], Peiguang Zhang[a], Zenghui Peng[a], Zhaoliang Cao[a], Quanquan Mu[a], Li Xuan[a]

[a] State Key Laboratory of Applied Optics, Changchun Institute of Optics, Fine Mechanics and Physics, Chinese Academy of Sciences, Changchun, Jilin 130033, China
[b] University of Chinese Academy of Sciences, Beijing 100039, China

ARTICLE INFO

Article history:
Received 9 September 2016
Received in revised form
28 November 2016
Accepted 2 January 2017
Available online 4 January 2017

Keywords:
Surface enhanced fluorescence
Flowerlike silver nanostructures
Liquid crystalline
Localized surface plasmon resonance
Organic distributed feedback laser

ABSTRACT

Highly effective surface-enhanced fluorescence substrates with roughened 3D flowerlike silver nanostructures were fabricated by electrodeposition in liquid crystalline template which is simple and controllable. Due to the localized surface plasmon resonance of silver nanostructures, the substrates were used as surface enhanced fluorescence substrates. The morphology and optical properties of the substrates were studied. The fluorescence experiments of the Rhodamine 6G on the substrates for different growth times were carried out and the best enhancement factor of 181 was achieved. Eight substrates with the same growth conditions were used to study the reproducibility of the substrate which shows that the fluctuations are within 9%. This substrate was used in organic distributed feedback lasers and the amplified spontaneous emission of poly(2-methoxy-5-(2′-ethyl-hexyloxy)-*p*-phenylenevinylene) was enhanced dramatically which means the reduced threshold and improved slope efficiency. Such easily fabricated flower-like silver nanostructure substrates with strong surface enhanced fluorescence effect and good reproducibility are good candidate for potential applications in optical imaging, biotechnology and material detections.

1. Introduction

Surface enhanced fluorescence (SEF) is a technique for enhancing the fluorescence intensity of fluorophores nearby the metallic surfaces [1–3]. Owing to its promising applications in optics [4,5] and biotechnology such as DNA detection [6], sensing [7] and diagnosis [8], there are more and more researchers devoted to SEF. Now it is widely accepted that the SEF effect mainly can be attributed to the localized surface plasmon resonance (LSPR) excited from the metallic nanostructures. The LSPR intensely modified the spectral properties of nearby fluorophores which is due to the coupling between the localized surface plasmon resonance band of the metallic structures and the characteristic bands of fluorophores including absorption and emission [2,9]. Thus, the SEF effect can be controlled by specially designed metallic nanostructures. The shapes, sizes and other morphology properties of the nanostructures have strong effect on the enhancement factor. Various shapes of metal nanostructures have been fabricated in the past several years such as nanoparticles, nanorods, dimers, fractal-like, etc [10–14]. Also many methods have been developed for synthesizing metal nanostructures, including the vapor deposition method, the e-beam lithography, the chemical reduction method and self-assembly of metal colloids [15–18]. However, powerful plasmon metallic nanostructures as SEF-active substrate with high enhancement factor as well as good reproducibility are still desirable in practical SEF techniques. It is found that 3D nanostructures such as flowerlike structures used as SEF substrates exhibit more favorable properties such as high enhancement factor owing to more 'hotspots' and enhanced local EM field than lower dimensional nanostructures [19,20]. Dong's group obtained good enhancement effect using flower-like silver nanostructures on Al substrate [13]. Chen's group using silver nanoparticle arrays obtained valid enhancement factor of 138 [10]. In 2015, Chris D.Geddes' group observed the basic fuchsin fluorescence enhancement factor is up to 7 fold using zinc substrates [21]. Substrates composed of flowerlike nanostructures on SEF with large enhancement factor are

* Corresponding author.
E-mail address: ycldahai@ciomp.ac.cn (C. Yang).

http://dx.doi.org/10.1016/j.apsusc.2017.01.010
0169-4332/

still desirable. However, there are still many problems to synthesize flowerlike nanostructures with complicated morphology such as complex production process, high cost, time consuming, poor reproducibility and so on, which limit the practical applications for the substrates. The SEF properties of substrates with large scale uniform flower-like nanostructures still need to be studied.

In this work, highly roughened 3D flowerlike silver nanostructures were fabricated experimentally on ITO (indium tin oxide) glass. The optical properties and SEF effects were studied. From the experiments of fluorescence with the substrates for different growth times, we have confirmed that the surface enhanced fluorescence effect is controllable and the best fluorescence enhancement factor of 181 is achieved. The broaden LSPR band of the flower-like silver nanostructures owing to its high anisotropy shape and couplings between each flowers makes it possible to achieve the SEF effect in wide spectrum range. Also, the stability of the flowerlike silver substrates is better than the flowerlike silver colloids which is because the flowerlike nanostructures on the substrates will not aggregate. We applied this substrate on organic distributed feedback (DFB) lasers [22–26] which is made from holographic polymer dispersed liquid crystal (HPDLC) transmission gratings with organic semiconductor poly(2-methoxy-5-(2′-ethyl-hexyloxy)-*p*-phenylenevinylene) (MEH-PPV). The fluorescence experiments of the organic semiconductor MEH-PPV were carried out and the enhancement factor of 41 was obtained. The intensity of ASE spectrum of MEH-PPV was enhanced dramatically which means the reduced threshold and improved slope efficiency of the laser [27,28].

2. Experiment

2.1. Materials

Anionic surfactant sodium bis (2-ethylhexyl) sulfosuccinate (AOT) (98 wt%), oil phase *p*-xylene (99 wt%) and silver nitrate (99 wt%) were purchased from Sigma-Aldrich Chemical Company. Rhodamine 6G (R6G) was purchased from J&K(China) which is a kind of very common fluorescence dye in the research field of surface enhanced fluorescence. The organic semiconducting MEH-PPV ($M_w \sim 10^5$) was obtained from Xi'an P-OLED Material Corporation and used as received. Deionized water was obtained from the Millipore Elixir 100 and the resistivity is over 18 MΩ cm. Silver foil (2.0 mm 99%) was from Alfa Aesar.

2.2. Fabrication of flower-like silver nanostructures

In this work, we use the liquid crystalline phase as the soft template to fabricate the flower-like silver nanostructures. The liquid crystalline phase was prepared according to the ternary phase diagram [29], consisting of the anionic surfactant sodium bis (2-ethylhexyl) sulfosuccinate (AOT), the oil phase *p*-xylene and water. The electrodeposition processes with different deposition times for various sizes and coverage ratio of flowerlike nanostructures were carried out. The details of the liquid crystalline preparation and electrodeposition are represented as follows. The liquid crystalline phase was prepared according to the ternary phase diagram mentioned above consisting of AOT, oil phase *p*-xylene and water which was replaced by $AgNO_3$ aqueous solution for the growth of silver flowers in this work. At first, the AOT was dissolved in the *p*-xylene with 1.4 M concentration. Then the aqueous 0.3 M $AgNO_3$ solution was added to the mixture drop by drop. After 2 h violent stirring, the mixture becomes to a clear liquid. The liquid crystalline phase was used as electrolyte in electrodeposition process. In the electrodeposition process, the silver foil (the anode) was mounted with the indium tin oxide (ITO) glass (the cathode, $15 \times 40\ mm^2$) to form a cell with 0.7 mm cell gap. The surface of ITO glass was very clean and smooth for collecting the flower-like silver nanostructures. The 3.0 V DC voltage was applied between the anode and cathode by a DC voltage-stabilized power supply at room temperature. When the deposition process was finished, the negative electrode ITO glass was softly washed by ethanol and dried by a gentle flow of N_2. Silver structures with different sizes can be obtained by controlling the deposition time.

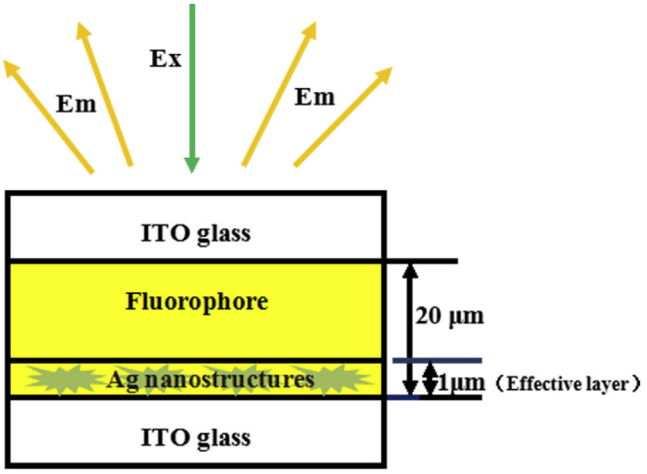

Fig. 1. The sandwich structure used in the surface enhanced fluorescence experiments. Ex and Em represent the excitation beam and fluorescence emitted. The thickness of the gap is about 20 μm with 1 μm effective layer.

2.3. Characterization

The morphology was observed by a field emission scanning electron microscope. The chemical constituent of the flower-like silver nanostructures was characterized by the energy dispersive spectrum. Extinction spectra of the flowerlike silver nanostructures were obtained from the Perkin Elmer Lambda 950 spectrometer with an integrating sphere.

2.4. Surface enhanced fluorescence effect experimental setups

To investigate the SEF effect of the flowerlike silver nanostructure substrates, the fluorescence emission spectra of R6G aqueous solution on the substrates were measured according to the method from Chris D.Geddes' group [30]. The R6G solution (2×10^{-5} M) was filled into the gap between the glass and the silver flower-like nanostructure film coated substrate which forms a sandwich structure. Fig. 1 shows the sandwich structure used in the SEF experiments. Ex and Em represent the excitation beam and fluorescence emitted, respectively. The thickness of the gap is 20 μm.

The experimental setups for surface enhanced fluorescence experiment are shown in Fig. 2(a). The R6G was excited by a solid state laser with 532 nm wavelength. A beam splitter was used to separate the exciting path and detection path. A 10× objective was used to focus the excitation beam and collect the fluorescence which was emitted nondirectionally. A notch filter was used to remove the excitation light from the collected fluorescence whose optical density was 6 at 532 nm. Then a fiber coupler focuses the fluorescence into the fiber. Ocean Optics USB 4000 spectrometer was employed to record the fluorescence spectra. Fig. 2(b) is the photograph of the experimental setups. The experiments were carried out at room temperature.

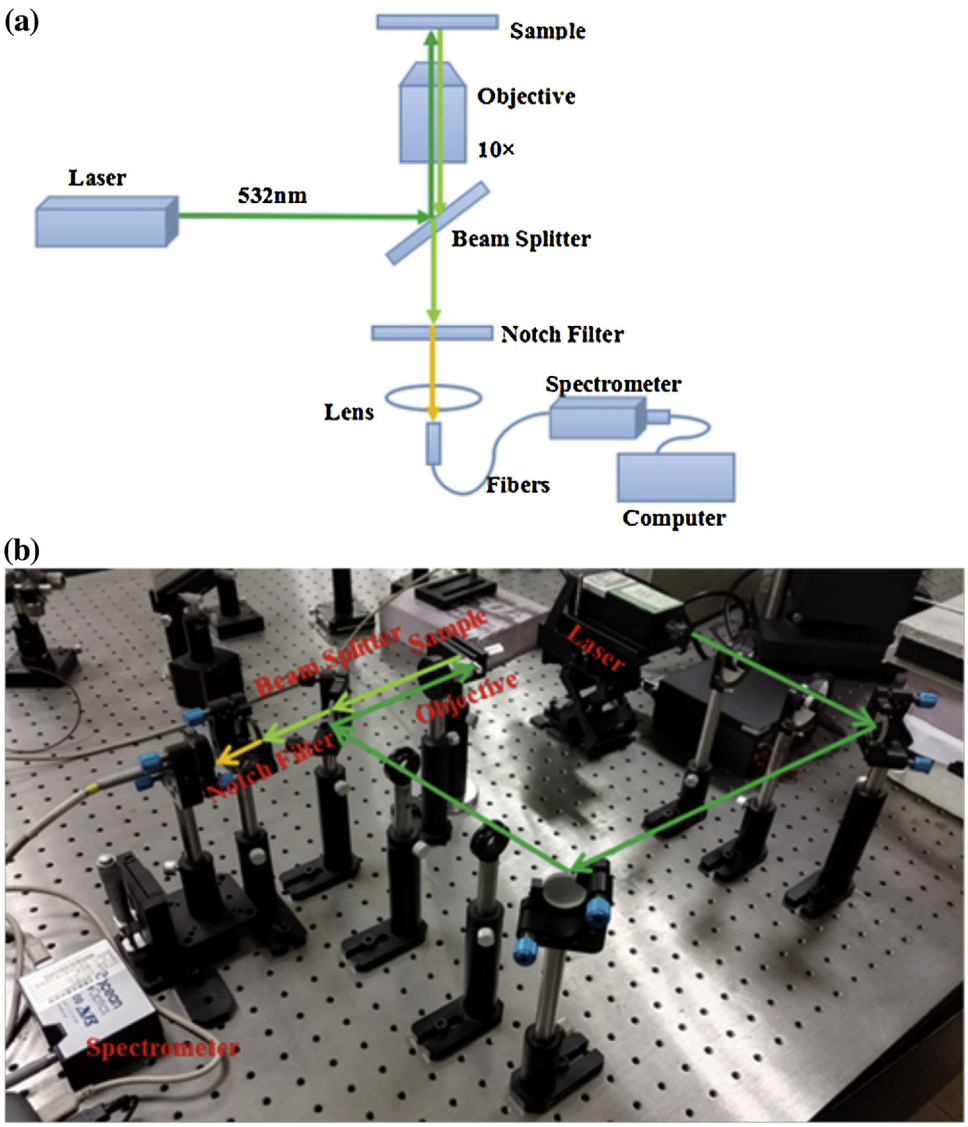

Fig. 2. Experimental setups for surface enhanced fluorescence experiments. The R6G was excited by a solid state laser with 532 nm wavelength. The exciting path and detection path was separated by the beam splitter. A notch filter was used to remove the excitation light from the collected fluorescence. Ocean Optics USB 4000 spectrometer was employed to record the fluorescence spectra. (a) is the diagram of experimental setups for surface enhanced fluorescence experiment (b) is the photograph of the experimental setups.

2.5. Application in organic distributed feedback lasers

2.5.1. Fluorescence enhancement of MEH-PPV

To investigate the SEF effect of MEH-PPV by the flowerlike silver nanostructure substrate, the fluorescence emission spectra of MEH-PPV chlorobenzene (CB) solution on the substrates were measured according to the method mentioned above. The concentration of MEH-PPV CB solution was 0.8 wt%. Absorption spectrum was obtained by UV-3101PC UV–vis-NIR scanning spectrophotometer.

2.5.2. ASE enhancement of MEH-PPV

To improve the intensity of output laser of the DFB lasers made from HPDLC transmission gratings with organic semiconductor MEH-PPV, the flowerlike silver nanostructure substrate was used. The MEH-PPV CB solution was filled into the gap between the glass and the silver flower-like nanostructure film coated substrate which forms a sandwich structure as Fig. 1 shows. The optical setups for investigating ASE properties of MEH-PPV are shown in Fig. 3. The frequency doubled pulsed Nd:YAG laser at 532 nm (1 Hz, 8 ns) was used as the pump source. The pump energy upon the device was 27 μJ monitored by an energy meter. The pump beam shaped by the cylindrical lens was incident on the sample from the normal direction of the cell. Output emission was collected by a spectrometer with a resolution of 0.3 nm.

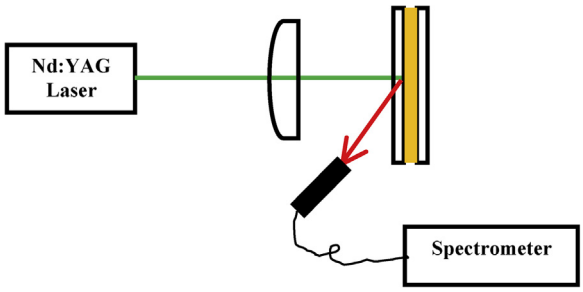

Fig. 3. The optical setups for investigating enhanced ASE properties of MEH-PPV. The frequency doubled pulsed Nd:YAG laser was used as the pump source. The pump beam shaped by the cylindrical lens was incident upon the sample to the normal of the cell. Output emission was collected by a spectrometer with a resolution of 0.3 nm.

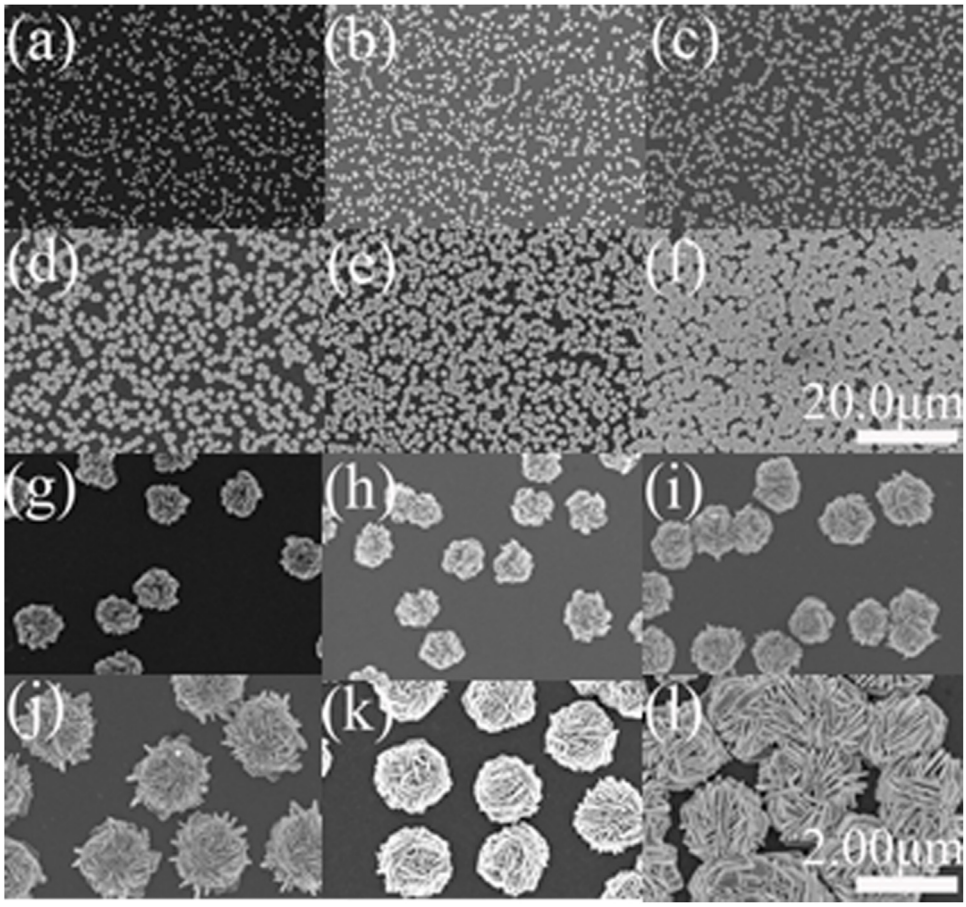

Fig. 4. FESEM images of the silver flower-like nanostructures for different growth times. (a)–(f) are top views with low magnification of the silver flowers for 10 min, 15 min, 0.5 h, 1.5 h, 2 h and 5 h growth times, respectively. (g)–(l) are the magnified images of (a)–(f), respectively. The two scale bars are 20.0 μm for (a)–(f) and 2.00 μm for (g)–(l).

3. Results and discussion

3.1. Morphology and constituent characterization

The morphology of the silver nanostructure substrates was observed by a field emission scanning electron microscope (FESEM). The size, morphology and coverage ratio of the silver nanostructures mainly depend on the growth time when the silver ion concentration is fixed. From the experiment, when the growth time is about 5 min, silver nanoparticles with uniform distribution were formed on the ITO glass substrate. When the growth time is more than 5 min, flowerlike silver nanostructures were obtained. The sizes and coverage ratio of silver flowers increase with growth time. Fig. 4 shows the images of flowerlike silver nanostructures with highly roughened surface obtained at room temperature for different growth times when the $AgNO_3$ concentration was 0.3 M. Fig. 4(a)–(f) are the FESEM images with low magnification of the silver flowers for 10 min, 15 min, 0.5 h, 1.5 h, 2 h, 5 h growth times respectively, which shows that coverage ratio of silver flowers increase with growth time and the obtained silver nanostructures are uniformly distributed in the surface of substrate in large scale. Actually, the silver flowers are uniform on the whole ITO glass substrate ($15 \times 40\,mm^2$) in our experiment and we believe that such uniform silver structures can be achieved in even larger scale. Fig. 4(g)–(l) are the magnified images of (a)–(f) respectively, from which we can see that the sizes of silver flowers are also uniform and increase with growth time. When the growth time is 10 min, the flower-like silver nanostructures with about 600 nm diameter are obtained. As time increases, the diameters become to 750 nm, 900 nm, 1.4 μm, 1.5 μm and 1.9 μm for 15 min, 0.5 h, 1.5 h, 2 h, 5 h growth times, respectively. Fig. 5(a) is the picture of single silver flower. The fabricated silver structure is quite like a rose composed of high density petals whose thickness is about 50 nm which increases with the growth time. Between the petals there are many horns and thin gaps. Fig. 5(b) and (c) are side views of the substrate from which we can see that the height of the flowers is about 700 nm, which also increases with growth time.

The energy dispersive spectrum (EDS) was performed to analyze the chemical constituent of the silver flowers (Fig. 5(d)). From the EDS result, peaks of silver, carbon and sulfur are observed. The dominant peak is for element silver, which addresses that the flower-like nanostructures are mainly composed of metallic silver. The peaks for carbon and sulfur can be attributed to the residuary AOT template in the sample. Only by the simple washing process, the template molecule cannot be all removed from the nanoscale space among the petals and flowers.

3.2. Extinction properties

As we know, the optical property such as localized surface plasmon resonance and surface enhanced fluorescence is influenced by metal nanostructures' morphology. So, the optical properties were studied before SEF effect. Extinction spectra of the flower-like silver nanostructures were measured from the Perkin Elmer Lambda 950 spectrometer with an integrating sphere. Fig. 6 shows the LSPR bands of flower-like silver nanostructures for 0.5 h (Fig. 6(a)), 1.5 h (Fig. 6(b)), 2 h (Fig. 6(c)) and 5 h (Fig. 6(d)) growth time, respectively. It is noted that the LSPR band is red-shifted and wider than sliver

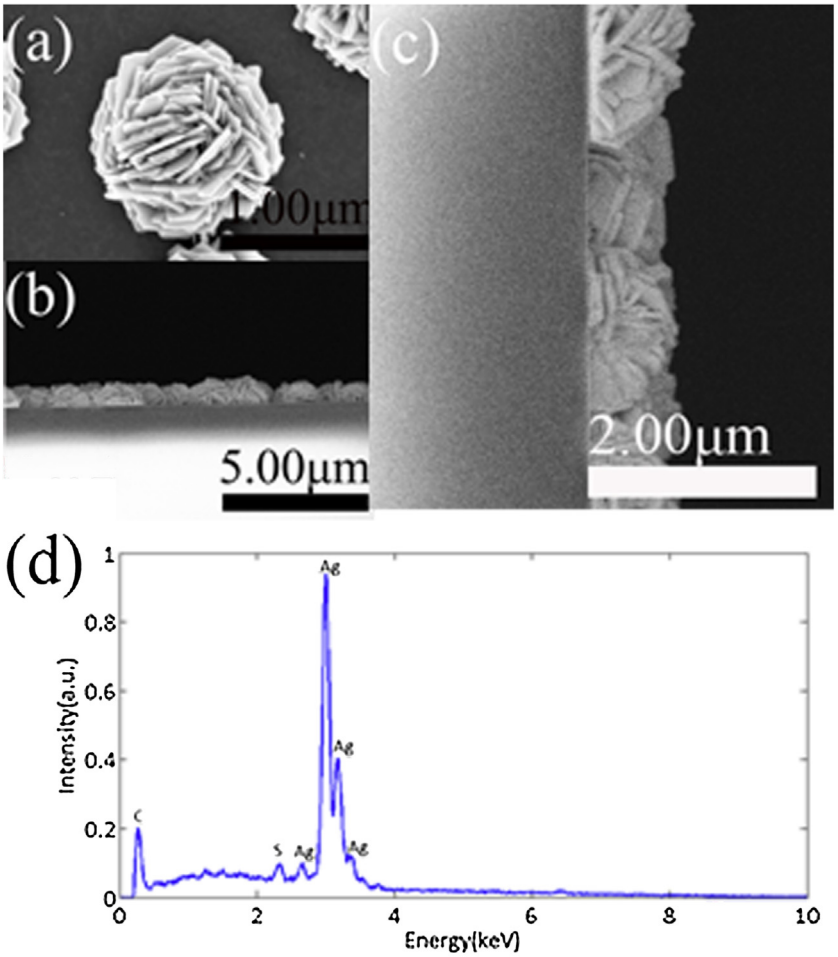

Fig. 5. Typical SEM morphology and energy dispersive spectrum of the silver flower-like nanostructures. (a) is the picture of single silver flower. (b) and (c) are the side views of the substrate. (d) is the energy dispersive spectrum of the silver flowers.

nanoparticles (not shown in this work) whose dipole resonance band is around 410 nm [31–33]. Several peaks at around 500 nm and 550 nm in the spectrum corresponding to higher-order multipole resonances were observed. As the growth time increases, peaks can be observed obviously in Fig. 6(b), which agrees with the Mie theory that anisotropic morphology can induce more LSPR bands [34]. Fig. 6(b) shows that when the growth time is 1.5 h, the bands around 650 nm and 480 nm are appeared corresponding to higher-order multipole resonances such as quadrupole and octupole resonance, respectively. The band which corresponding to dipole resonance red-shifted to infrared region compared to silver flowers obtained for 0.5 h and becomes more enhanced. Furthermore, Fig. 6(c) and (d) shows that plasmon resonance is more intense with the growth time increases in which the enhancement of dipole resonance dominates the increase.

According to the Mie theory, for spherical Ag nanoparticles which is much smaller than the wavelength of light, the size satisfies "quasistatic" limit that means all the electrons in the particle experience the same phase of the incident electromagnetic field [35]. In this case, only the dipole plasmon resonance is excited. As the size of particle increases to similar with wavelength of light, electrons of particles experience different phase of the incident electromagnetic field which is called phase retardation effects [36,37]. In this case, higher order multipolar plasmon modes are excited at shorter wavelengths than the dipole plasmon mode in the particle's extinction spectrum. Otherwise, phase retardation effects lead to obvious red-shifting and broadening of the dipole resonance [38]. From the study of Feng Zhang, for silver particle with 400 nm diameter, the higher-order multipolar plasmon resonance are appeared at around 613 nm, 510 nm and 430 nm and the dipole resonance red-shifts to 820 nm [39]. For our flowerlike silver structures, as the growth time increases, the dipole resonance is red-shifted from 670 nm to near infrared. The higher-order multipolar plasmon resonance appeared. Considering the SEM photos shown before, as the growth increases, the size of silver flower are increased. According to the theory mentioned above, the similar phenomena appeared on the extinction spectra. Also, coupling between different nanoslices which constitute the silver flowers also broaden the resonance bands. Moreover, the increasing of the nanostructures' coverage ratio leads to the coupling between different flowers, which broaden the LSPR band, too. The LSPR spectra achieved can be attributed to the complicated shape of the silver flowers and the increased coverage ratio, which makes the sliver flowerlike nanostructures a good candidate for surface enhanced fluorescence.

The highly anisotropic shape of these silver nanostructures and coupling between nanostructures enormously influences the optical properties such as LSPR and SEF. The shape of the nanostructures determines the position of LSPR bands. According to the works of C. McDonagh's group [40] and Joseph R. Lakowicz's group [41], when the positions of absorption spectrum band and emission spectrum band of the fluorophores are overlapped with the LSPR band, the effect of surface enhanced fluorescence is the best. So the broad LSPR band is favorable for the SEF effect.

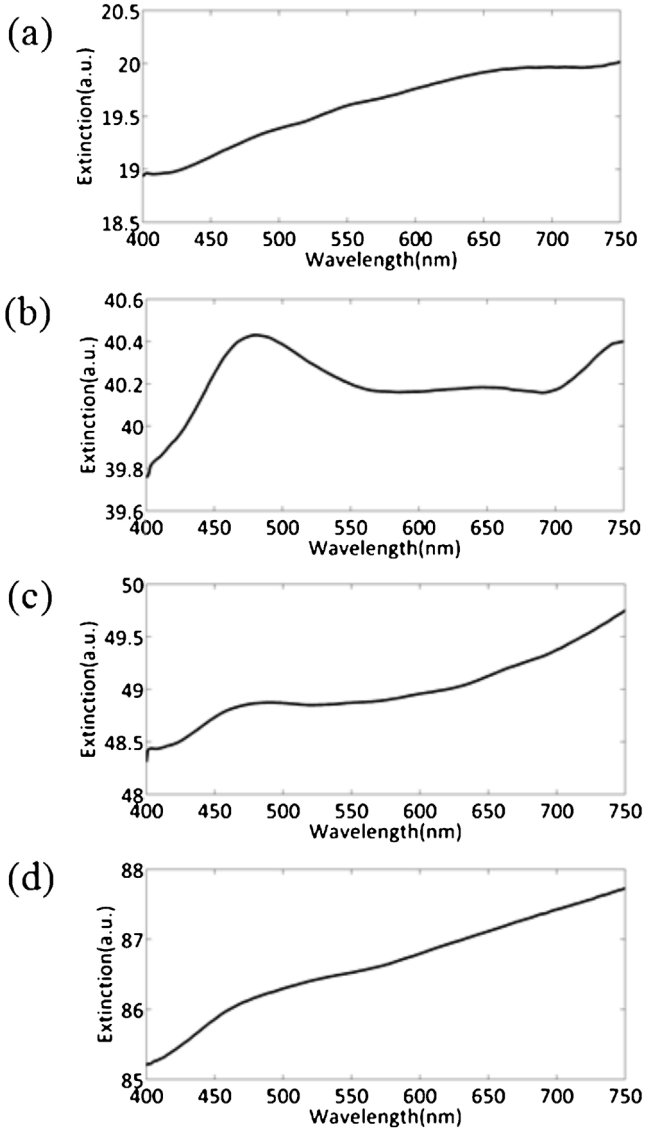

Fig. 6. The measured extinction spectra of silver flower-like nanostructure substrates with different growth time. (a–d) are the substrates for 0.5 h, 1.5 h, 2 h, 5 h growth time, respectively.

3.3. Surface enhanced fluorescence effect of R6G

The fluorescence spectra of R6G aqueous solution on the substrates are shown in Fig. 7. Curve a–e represent fluorescence from silver flower substrates of 0.5 h, 1 h, 1.5 h, 2 h and 5 h growth time respectively, and curve r is for glass substrate without silver flowers which is used as reference curve. We can see that the fluorescence signals of R6G are obviously enhanced by the flowerlike silver nanostructure substrates. The intensity of the fluorescence is much stronger than that on the glass substrate. The enhancement effect can be described by the factor (E_f) as follows

$$E_f = I_{Ag-substrate}/I_{reference} \quad (1)$$

where $I_{Ag-substrate}$ is the fluorescence intensity of R6G on the substrates with flowerlike silver nanostructures and $I_{reference}$ is the fluorescence intensity on the glass substrate. It can be seen that the enhancement factor increases with the growth time and the maximum value is achieved by the substrate of 5 h growth time. The best SEF intensity of 5 h growth time substrate was about 10.0 times higher than that on the glass substrate. It decreases to 7.5,

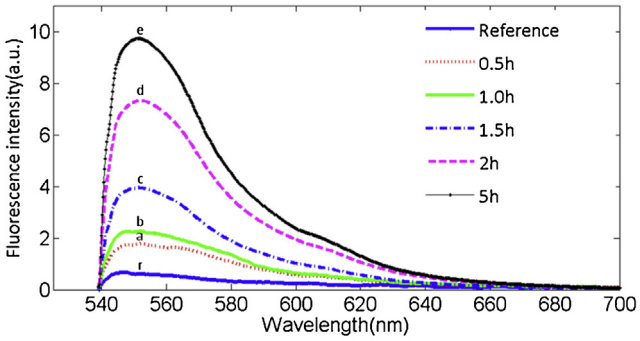

Fig. 7. Fluorescence spectra of R6G for substrates with different growth time. Curve a–e are for substrates of 0.5 h, 1.0 h, 1.5 h, 2 h and 5 h growth time respectively. Curve r is for glass substrate as reference.

4.0, 2.5 and 2.0 for 2 h, 1.5 h, 1 h and 0.5 h growth time substrates, respectively. However, according to the work of Chris D.Geddes' group [30], the SEF effect which originates from the interaction between the fluorophore and metallic surface only takes place in the space less than 20 nm from the metallic surface. That is to say the real effective enhancement factor is much larger than the observed value. In this work, the thickness of the flower-like silver nanostructure layer is about 1 μm and the cell gap is about 20 μm. In other words, the observed 10.0 times enhancement originates only from the 1 μm effective layer of the total 20 μm solution, the rest 19 μm solution are not enhanced. The correction calculation is necessary. We assume that the intensity of not enhanced part is Y per micrometer, while the enhanced part is X per micrometer. The total intensity equals to X plus 19Y which also equals to 10 × 20Y. The result is X equals to 181Y. So the real effective enhancement factor is about 181. In the same way, the effective enhancement factor are about 131, 62, 32 and 22 for 2 h, 1.5 h, 1 h and 0.5 h growth time substrates, respectively. In order to investigate the reliability of the corrected calculation, the cell with 60 μm gap was fabricated. After the same corrected calculation, the enhancement factors of 60 μm cell is about 175 which agrees well with 20 μm (181) cell mentioned above. So we think the corrected calculation we used is available for the effective enhancement factors in this work.

The spectra reproducibility of the flowerlike silver substrates was also studied. We fabricated eight substrates with the same growth conditions. The enhancement effects of each substrate are measured. Fig. 8(a) shows the results. We can see that the enhancement factors fluctuate around 180. Considering the process of the experiments, we think the fluctuation may come from the difference of substrates and the different cell gaps especially. But, the fluctuations are still within 9%. Fig. 8(b) shows the spectra for eight substrates and the shapes are very similar.

Fluorescence is a character for a material including two processes which are absorption and emission of light. The two processes were quantified by excitation efficiency and fluorescence quantum yield, respectively. According to the Jablonski diagram, the final fluorescence emission intensity is determined by the product of the two factors mentioned above. Excitation efficiency is influenced by the intensity of excitation light and fluorescence quantum yield is determined by the radiative and nonradiative decay rates [1]. Surface enhanced fluorescence is an approach for enhancing the fluorescence intensity of fluorophores nearby the metallic surfaces which due to the localized surface plasmon resonance from collective oscillation of electrons of the noble metal nanostructures. The enhancement effect could be attributed to three competing effects. Firstly, local field enhancement on the surface of metal nanostructures enhanced excitation efficiency. Secondly, surface plasmon coupled fluorescence emission causes increase of radiative decay rate, which

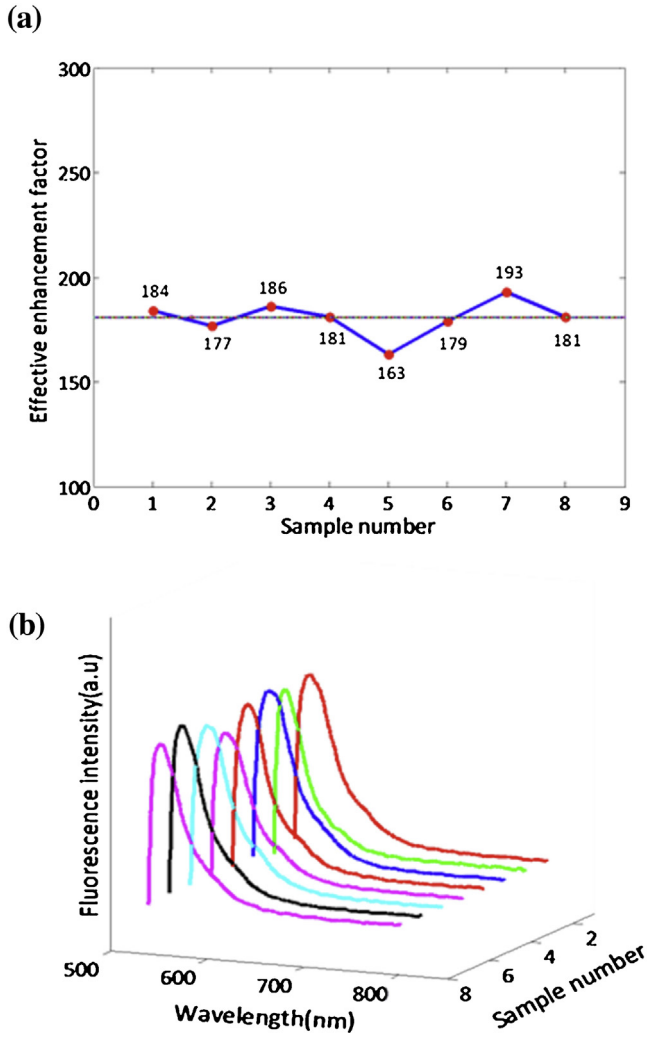

Fig. 8. The enhancement effects of eight substrates with the same growth conditions. (a) shows the fluctuation of the effective enhancement factors of eight different substrates with the same growth conditions. (b) is the picture of spectra of fluorophores for the eight flower-like silver substrates.

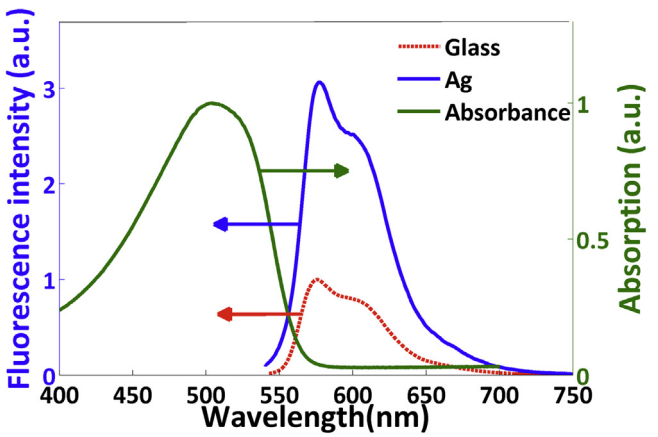

Fig. 9. The spectroscopic properties of the MEH-PPV CB solution on different substrates. The green curve is normalized absorption spectrum. The red and blue curves are fluorescence spectra of MEH-PPV CB solution without and with silver flower nanostructure substrates, respectively. (For interpretation of the references to color in this figure legend, the reader is referred to the web version of this article.)

leads to increased quantum yield resulting in the fluorescence enhancement. Thirdly, the non-radiative energy transfer from the fluorophores to metal nanostructures leads to increased non-radiative decay rate resulting in fluorescence quenching [1,2,42,43]. The enhanced fluorescence emission of R6G near silver flowerlike nanostructures can be attributed to the increased excitation efficiency and quantum yield rates which originate from the enhanced local field and increased radiative decay rate of the fluorophores. The enhanced local field leads to the enhanced excitation rates, which is determined by the level of overlap between the LSPR bands and the excitation band of fluorophores. The increased radiative decay rate improves the quantum yield rates of the fluorophores. The enhanced fluorescence intensity is the cooperative effect of the aspects mentioned above. However, quantum yield of R6G without metal structures is already over 94% [44]. In our study, the measured extinction spectra of silver flowers consist of several localized surface plasmon resonance and each LSPR band is the superposition of many plasmon resonances. The complex morphology of the flower-like nanostructures and the coupling between nanostructures lead to the wide LSPR bands which achieves high level overlap between the LSPR band and the excitation band of fluorophores. Furthermore, the flowerlike silver structures are made up of high density petals, which provide many horns on the petals and thin gaps between adjacent petals which is favorable for generating 'hotspots'. The increase of the fluorescence intensity with the growth time can be attributed to the increasing surface area and more complicated morphology of silver nanostructures which will lead to stronger localized fields and more coupling with fluorophores. So the surface enhanced fluorescence effect can be controlled by changing the growth time.

3.4. Application in organic distributed feedback lasers

3.4.1. Surface enhanced fluorescence effect of MEH-PPV

The spectroscopic properties of the MEH-PPV CB solution on different substrates are shown in Fig. 9. The green curve is normalized absorption spectrum of MEH-PPV CB solution. The absorption of the solution peak is at around 503 nm and strong absorption at the exciting wavelength of 532 nm can also be observed. The red curve is fluorescence spectrum of MEH-PPV CB solution without silver flower nanostructure substrate which is used as the reference and the green curve is fluorescence spectrum with silver flower nanostructure substrate. The photoluminescence (PL) spectrum peak is at around 576 nm and with shoulder near 607 nm. The spectra overlap (from 541 nm to 561 nm) between PL bands and absorption which means that self-absorption loss is significant and lasing action cannot be obtained at this region. We can see that the fluorescence signals of MEH-PPV CB solution are obviously enhanced by the flowerlike silver nanostructure substrate. The enhancement factor calculated by the method mentioned above is 41.

3.4.2. ASE enhancement of MEH-PPV

The results of ASE enhancement are shown in Fig. 10. Fig. 10(a) and (b) are the photos of the devices without and with flowerlike silver nanostructure substrates respectively pumped by the pulsed laser (532 nm). From Fig. 10(a) and (b), we can see that the color of two cells are slight different, (b) contains more red component than (a) which means that the enhanced ASE emission contains more long wavelength band. Fig. 10(c) shows the ASE spectra of MEH-PPV CB solution with (bule curve) and without (red curve) silver nanostructure substrates, respectively. The green curve in Fig. 10(c) is the normalized fluorescence spectrum. Only one peak at around 569 nm was detected without silver structure while two peaks at around 569 nm and 610 nm were detected with silver nanostructures. From Fig. 10(c) we can see that, the intensity of the peak at around 569 nm is enhanced dramatically. The peak around 610 nm did not appear in the red curve. In the

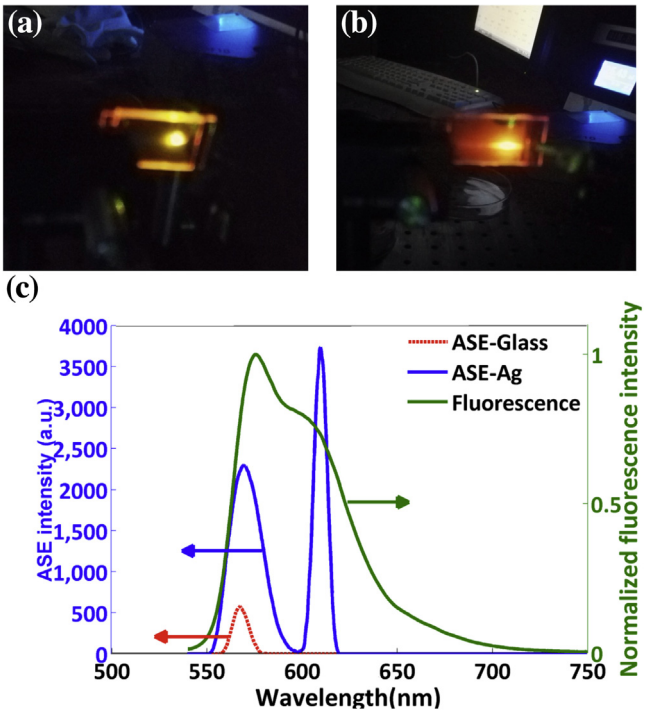

Fig. 10. The results of enhanced ASE properties of MEH-PPV CB solution. (a) and (b) are the photos of the cells without and with flowerlike silver nanostructure substrates pumped by the pulsed laser (532 nm), respectively. (c) the ASE spectra of MEH-PPV CB solution with (bule curve) and without (red curve) silver nanostructure substrates. The green curve is the normalized fluorescence spectrum. (For interpretation of the references to color in this figure legend, the reader is referred to the web version of this article.)

experiment we also find that when the emission was detected at the side of the device with the silver nanostructures cell, there is only one peak with a strong intensity at around 610 nm and its bandwidth is about 0.5 nm which we think is a phenomenal related to random lasers (not shown). According to the study before, ASE spectrum can be used for predicting the laser efficiency and threshold [27,28], increasing the intensity of ASE will lead to increased slope efficiency and decreased threshold. So, our flowerlike silver nanostructure substrates are good candidate for application in the organic distributed feedback lasers.

4. Conclusions

In this work, we have demonstrated the highly effective surface enhanced fluorescence substrate with 3D flower-like silver nanostructures fabricated in liquid crystalline phase experimentally. Wide LSPR band is achieved due to the complex morphology and the coupling between silver flowers. With the fluorescence experiments of R6G, enhancement factor of 181 is achieved. Eight substrates with the same growth conditions were used to study the reproducibility of the substrate and the fluctuations of enhancement effect are within 9%. The substrates were applied on organic distributed feedback lasers made from HPDLC and the enhanced ASE of organic semiconductor MEH-PPV CB solution was investigated. The intensity of ASE was enhanced dramatically which means the reduced threshold and improved slope efficiency of the laser. Such highly effective, good reproducible and easily fabricated SEF substrates are a good candidate for many potential SEF applications such as optical imaging, biotechnology and material detections.

Acknowledgment

This work is supported by the National Natural Science Foundation of China with grant numbers 11204299, 61205021 and Youth Innovation Promotion Association CAS.

References

[1] E. Fort, S. Grésillon, Surface enhanced fluorescence, J. Phys. D: Appl. Phys. 41 (2008) 013001.
[2] J.R. Lakowicz, Radiative decay engineering 5: metal-enhanced fluorescence and plasmon emission, Anal. Biochem. 337 (2005) 171–194.
[3] J.R. Lakowicz, K. Ray, M. Chowdhury, H. Szmacinski, Y. Fu, J. Zhang, K. Nowaczyk, Plasmon-controlled fluorescence: a new paradigm in fluorescence spectroscopy, Analyst 133 (2008) 1308–1346.
[4] K. Aslan, J.R. Lakowicz, C.D. Geddes, Plasmon light scattering in biology and medicine: new sensing approaches, visions and perspectives, Curr. Opin. Chem. Biol. 9 (2005) 538–544.
[5] Q. Sun, K. Ueno, H. Yu, A. Kubo, Y. Matsuo, H. Misawa, Direct imaging of the near field and dynamics of surface plasmon resonance on gold nanostructures using photoemission electron microscopy, Light Sci. Appl. 2 (2013) e118.
[6] J. Malicka, I. Gryczynski, J.R. Lakowicz, DNA hybridization assays using metal-enhanced fluorescence, Biochem. Biophys. Res. Commun. 306 (2003) 213–218.
[7] N. Li, A. Tittl, S. Yue, H. Giessen, C. Song, B. Ding, N. Liu, DNA-assembled bimetallic plasmonic nanosensors, Light Sci. Appl. 3 (2014) e226.
[8] S. Guo, S. Dong, E. Wang, A general method for the rapid synthesis of hollow metallic or bimetallic nanoelectrocatalysts with urchinlike morphology, Chem. Eur. J. 14 (2008) 4689–4695.
[9] Y. Zhang, A. Dragan, C.D. Geddes, Wavelength dependence of metal-enhanced fluorescence, J. Phys. Chem. C. 113 (2009) 12095–12100.
[10] B. Yang, N. Lu, D. Qi, R. Ma, Q. Wu, J. Hao, X. Liu, Y. Mu, V. Reboud, N. Kehagias, C.M.S. Torres, F.Y.C. Boey, X. Chen, L. Chi, Tuning the intensity of metal-enhanced fluorescence by engineering silver nanoparticle arrays, Small 6 (2010) 1038–1043.
[11] H. Zheng, L. Xu, Z. Zhang, J. Dong, S. Chen, X. Zhang, Fluorescence enhancement of acridine orange in a water solution by Au nanoparticles, Sci. China Phys. Mech. Astron. 53 (2010) 1799–1804.
[12] K. Aslan, Z. Leonenko, J.R. Lakowicz, C.D. Geddes, Fast and slow deposition of silver nanorods on planar surfaces: application to metal-enhanced fluorescence, J. Phys. Chem. B 109 (2005) 3157–3162.
[13] J. Dong, H. Zheng, X. Yan, Y. Sun, Z. Zhang, Fabrication of flower-like silver nanostructure on the Al substrate for surface enhanced fluorescence, Appl. Phys. Lett. 100 (2012) 051112.
[14] X. Fan, W. Zheng, D.J. Singh, Light scattering and surface plasmons on small spherical particles, Light Sci. Appl. 3 (2014) e179.
[15] M. Sackmann, S. Bom, T. Balster, A. Materny, Nanostructured gold surfaces as reproducible substrates for surface-enhanced Raman spectroscopy, J. Raman. Spectrosc. 38 (2007) 277–282.
[16] P.S. Kumar, I. Pastoriza-Santos, B. Rodriguez-Gonzalez, F.J.G. de Abajo, L.M. Liz-Marzan, High-yield synthesis and optical response of gold nanostars, Nanotechnology 19 (2008) 015606.
[17] A.V. Whitney, J.W. Elam, P.C. Stair, R.P. Van Duyne, Toward a thermally robust operando surface-enhanced Raman spectroscopy substrate, J. Phys. Chem. C 111 (2007) 16827–16832.
[18] A. Mohanty, N. Garg, R. Jin, A universal approach to the synthesis of noble metal nanodendrites and their catalytic properties, Angew. Chem. Int. Ed. 49 (2010) 4962–4966.
[19] J. Dong, S. Qu, Z. Zhang, M. Liu, G. Liu, X. Yan, H. Zheng, Surface enhanced fluorescence on three dimensional silver nanostructure substrate, J. Appl. Phys. 111 (2012) 093101.
[20] H. Xia, W. Xiao, M. Lai, L. Lu, Facile synthesis of novel nanostructured MnO2 thin films and their application in supercapacitors, Nanoscale Res. Lett. 4 (2009) 1035–1040.
[21] H.B. Hamo, J. Karolin, B. Mali, A. Kushmaro, R. Marks, C.D. Geddes, Metal-enhanced fluorescence from zinc substrates can lead to spectral distortion and a wavelength dependence, Appl. Phys. Lett. 106 (2015) 081605.
[22] T. Woggon, S. Kinkhammer, U. Lemmer, Compact spectroscopy system based on tunable organic semiconductor lasers, Appl. Phys. B 99 (2010) 47–51.
[23] Y. Yang, G.A. Turnbull, I.D.W. Samuel, Sensitive explosive vapor detection with polyfluorene lasers, Adv. Funct. Mater. 20 (2010) 2093–2097.
[24] J. Clark, G. Lanzani, Organic photonics for comminications, Nat. Photon. 4 (2010) 438–446.
[25] V.K.S. Hsiao, C. Lu, G.S. He, M. Pan, A.N. Cartwright, P.N. Prasad, High contrast switching of distributed feedback lasing in dye-doped H-PDLC transmission grating structures, Opt. Express 13 (2005) 3787.
[26] Y.J. Liu, X.W. Sun, H.I. Elim, W. Ji, Effect of liquid crystal concentration on the lasing properties of dye-doped holographic polymer-dispersed liquid crystal transmission gratings, Appl. Phys. Lett. 90 (2007) 011109.
[27] P.K. Kevin, B. Colin, L. Stephen, J.B. Werner, Z.H. Fryad, R. Henning, P. Annett, T. Hartwig, H. Hansheinrich, Amplified spontaneous emission and optical gain spectra from stilbenoid and phenylene rinylene derivative model compounds, J. Appl. Phys. 86 (1999) 6155.

[28] N. Tsutsumi, T. Kawahira, W. Sakai, Amplified spontaneous emission and distributed feedback lasing from a conjugated compound in various polymer materices, Appl. Phys. Lett. 83 (2003) 2533.
[29] P. Ekwall, L. Mandell, K. Fontell, Solubilization in micelles and mesophases and the transition from normal to reversed structures, Mol. Cryst. Liquid Cryst. 8 (1969) 157–213.
[30] Y. Zhang, A. Dragan, C.D. Geddes, Metal-enhanced fluorescence from tin nanostructured surfaces, J. Appl. Phys. 107 (2010) 024302.
[31] P.K. Jain, K.S. Lee, I.H. El-Sayed, M.A. El-Sayed, Calculated absorption and scattering properties of gold nanoparticles of different size shape, and Composition: applications in biological imaging and biomedicine, J. Phys. Chem. B 110 (2006) 7238–7248.
[32] E. Petryayeva, U.J. Krull, Localized surface plasmon resonance: nanostructures, bioassays and biosensing—a review, Anal. Chim. Acta 706 (2011) 8–24.
[33] C.J. Murphy, T.K. Sau, A.M. Gole, C.J. Orendorff, J. Gao, L. Gou, S.E. Hunyadi, T. Li, Anisotropic metal nanoparticles: synthesis, assembly, and optical applications, J. Phys. Chem. B 109 (2005) 13857–13870.
[34] R. Boyack, E.C. Le Ru, Investigation of particle shape and size effects in SERS using T-matrix calculations, Phys. Chem. Chem. Phys. 11 (2009) 7398–7405.
[35] C.F. Bohren, D.R. Huffman, Absorption and Scattering of Light by Small Particles, John Wiley & Sons, 2008.
[36] D.D. Evanoff, G. Chumanov, Synthesis and optical properties of silver nanoparticles and arrays, ChemPhysChem 6 (2005) 1221–1231.
[37] M. Meier, A. Wokaun, Enhanced fields on large metal particles: dynamic depolarization, Opt. Lett. 8 (1983) 581–583.
[38] A. Wokaun, J. Gordon, P. Liao, Radiation damping in surface-enhanced Raman scattering, Phys. Rev. Lett. 48 (1982) 957.
[39] F. Zhang, P. Chen, L. Zhang, S.-C. Mao, L. Lin, Y.-G. Tang, J.-C. Cui, X.-D. Qi, J.-H. Yang, Y.-F. Ma, Enhancement of Raman scattering by field superposition of rough submicrometer silver particles, Appl. Phys. Lett. 100 (2012) 173103.
[40] O. Stranik, H.M. McEvoy, C. McDonagh, B.D. MacCraith, Plasmonic enhancement of fluorescence for sensor applications, Sens. Actuators B-Chem. 107 (2005) 148–153.
[41] J.R. Lakowicz, B. Shen, Z. Gryczynski, S. D'Auria, I. Gryczynski, Intrinsic fluorescence from DNA can Be enhanced by metallic particles, Biochem. Biophys. Res. Commun. 286 (2001) 875–879.
[42] P. Bharadwaj, L. Novotny, Spectral dependence of single molecule fluorescence enhancement, Opt. Express 15 (2007) 14266–14274.
[43] W. Ge, X. Zhang, M. Liu, Z. Lei, R. Knize, Y. Lu, Distance dependence of gold-enhanced upconversion luminescence in Au/SiO 2/Y 2 O 3: Yb 3+, Er 3+ nanoparticles, Theranostics 3 (2013) 282–288.
[44] N. Trong Nghia, D. Thi Hue, N. Dinh Hoang, V. Duong, D. Quang Hoa, T. Hong Nhung, N. Thi Ha Lien, Enhanced absorption and fluorescence of gold nanoclusters using initial alkali concentrations, Appl. Phys. Express 9 (2016) 022001.